Why do veins appear blue? A new look at an old question

Alwin Kienle, Lothar Lilge, I. Alex Vitkin, Michael S. Patterson, Brian C. Wilson, Raimund Hibst, and Rudolf Steiner

We investigate why vessels that contain blood, which has a red or a dark red color, may look bluish in human tissue. A CCD camera was used to make images of diffusely reflected light at different wavelengths. Measurements of reflectance that are due to model blood vessels in scattering media and of human skin containing a prominent vein are presented. Monte Carlo simulations were used to calculate the spatially resolved diffuse reflectance for both situations. We show that the color of blood vessels is determined by the following factors: (i) the scattering and absorption characteristics of skin at different wavelengths, (ii) the oxygenation state of blood, which affects its absorption properties, (iii) the diameter and the depth of the vessels, and (iv) the visual perception process.

1. Introduction

The bluish appearance of human veins has spawned many discussions, for it seems at odds with the dark red color of venous blood. In the literature this issue has been treated only qualitatively[1] to our knowledge. As we are dealing with photon propagation and remittance from skin, it is worth noting that most human tissues are highly scattering in the visible and near-infrared regions of the spectrum, making the scattering process 100–1000 times more probable than the absorption process.[2] The absorption of tissue can vary by several orders of magnitude, depending on the concentration and molar absorption coefficients of specific chromophores and the wavelength used. Moreover, tissues are heterogeneous and are often composed of different structures having different optical properties, as is the case for human skin.[3] Therefore, describing the penetration, absorption, scattering, and remittance of light at different wavelengths and hence the color of the skin is a complex task. Understanding light transport in tissue is the key to understanding the color of blood vessels in skin.

Describing photon propagation in tissue using Maxwell equations[4] has had limited success in deriving useful expressions for relevant quantities such as spatially resolved reflectance from tissue and photon distribution in the tissue. Instead, the transport equation has been used successfully.[5] This equation regards light as a collection of particles and deals only with intensities. Wave effects such as coherent backscattering[6] are not considered. In this paper we use Monte Carlo simulations to calculate the photon propagation in tissue, because this technique is capable of handling complex geometries.

To model the problem *in vitro,* experiments were conducted using a fat emulsion to represent a highly scattering and weakly absorbing medium and a cylindrical glass tube filled with blood to represent the blood vessel. Oxygenated as well as deoxygenated blood was used in the phantom work. *In vivo* measurements were also made on a human vein in the ball of the thumb. Measurements were performed at different wavelengths using filtered light from an arc lamp. The diffusely reflected light was

A. Kienle, R. Hibst, and R. Steiner are with the Institut für Lasertechnologien in der Medizin, Helmholtzstrasse 12, 89081 Ulm, Germany. L. Lilge, I. A. Vitkin, and B. C. Wilson are with the Department of Clinical Physics, Ontario Cancer Institute/Princess Margaret Hospital, University of Toronto, 500 Sherbourne Street, Ontario M4X 1K9, Canada. M. S. Patterson is with the Department of Medical Physics, Hamilton Regional Cancer Centre, 699 Concession Street, Hamilton, Ontario L8V 1C3, Canada.

Received 3 March 1995; revised manuscript received 28 September 1995.

0003-6935/96/071151-10$06.00/0

imaged onto a CCD camera to quantify the intensity of the emitted photons at positions above and beside the vessel. The measurements were compared to Monte Carlo simulations using the known optical coefficients of the tissue phantoms and published optical properties of human blood to check the experimental apparatus and the Monte Carlo calculations for this problem. For the *in vivo* measurements the Monte Carlo simulations were applied to estimate the optical coefficients of skin. Using these parameters the remission and hence the color of the vessels were computed for different depths and diameters of the vessels.

For a complete description of color as perceived by the human observer, the spectral sensitivity and the physiology of the eye need to be considered. Textbooks often employ standard spectrophotometric methods to determine the color of an object based on measurements of the reflected intensities at three different wave bands correlated to the sensitive bands in the retina of the eye. However, this does not correspond to how we see the object. Even convolution of the remitted intensity with the tristimulus response of the eye does not explain the perceived colors correctly.[7] Beginning in the late 1950's, Edwin Land proposed that higher-order mental processing be involved in color vision, and his pioneering work on this subject established the retinex (retina plus cortex) theory. We use this theory together with experimental results and Monte Carlo simulations to show that a vein or an artery looks bluish/turquoise when it is a certain depth below the surface of a scattering medium.

Besides the pure scientific point of view, this research has some potential for clinical applications because, from the color of a vessel taking into account its apparent diameter and probable oxygen saturation, its depth can be estimated. One possibility to profit from this information is the differentiated treatment of vessel malformations with laser radiation. For example, if one knows the depth of the vessel the applied wavelength can be chosen to obtain the best therapeutical success.

2. Theory

A. Monte Carlo Simulation

One can normally apply the transport theory to describe photon propagation in tissue using four optical parameters: (i) scattering coefficient μ_s, (ii) absorption coefficient μ_a, (iii) scattering anisotropy factor g, and (iv) refractive index n. In most tissue types refractive index n is approximately 1.4.[8] This value is used in this paper for all tissue sorts including the vessel, although blood has a somewhat smaller refractive index.[5] However, this approximation does not strongly influence light propagation. (Using $n = 1.33$ for blood, the probability of reflection of the photons, which are perpendicularly incident onto the boundary between blood and the surrounding tissue, is less than 0.001.) As a consequence of the approximation the Fresnel reflection at the vessel boundary does not have to be calculated. One can solve the transport equation with Monte Carlo simulations[9,10] by tracing individual photon histories in which the scattering and absorption events can be determined by random sampling from known probability distributions.

Figure 1 shows the geometry for the Monte Carlo calculations in this study. The photons are incident perpendicular to the optically turbid medium. A cylindrical tube with diameter d at a depth a under the surface representing the blood vessel is placed in the light scattering medium that represents the skin. The surrounding medium is chosen to be infinite in the x, y, and positive-z directions, whereas the cylindrical tube is infinite in the y direction. In the experiment the incident beam is elliptical with an area of approximately 16 cm^2. For the calculations the incident beam was square with a lateral length $b = 4$ cm. This approximation does not influence the results noticeably because the beam diameter is much larger than the vessel diameter and the average penetration depth of the photons. With the Monte Carlo program one can simulate a line source and obtain the results for a square beam by applying a convolution technique. In this way the calculations are accelerated. The incident beam in the Monte Carlo program is chosen as a line source from $x = -b/2$ to $x = b/2$ along the x axis. The x and y coordinates of the locations of the remitted photons of the considered area are stored in a two-dimensional array $\chi(x, y)$. Then $\chi(x, y)$ is convolved with the beam profile in the y direction $S(y)$, which is a step function θ from $y = -b/2$ to $y = b/2$: $S(y) = S_0[\theta(y + b/2) - \theta(y - b/2)]$, to calculate the remission $R(x, y)$ of the photons for the square beam. S_0^{-1} equals the number of incident photons per pixel area of the two-dimensional array, and $R(x, y)$ is the absolute remission, which means the number of remitted photons divided through the number of incident photons:

$$R(x, y) = \int_{-\infty}^{\infty} S(y - y')\chi(x, y')\mathrm{d}y'. \qquad (1)$$

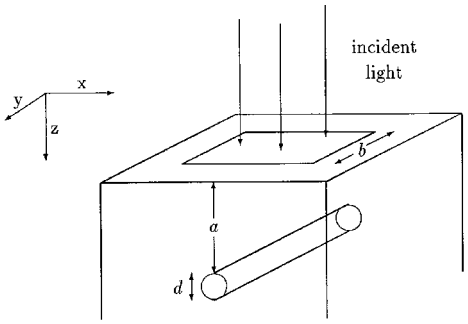

Fig. 1. Geometry of the model that was used in the Monte Carlo simulations.

For the central line of the reflectance image we get

$$R(x, y = 0) = S_0 \int_{-b/2}^{b/2} \chi(x, y')\mathrm{d}y'. \tag{2}$$

Thus, because from the Monte Carlo simulations one has χ in the form of an array, the integral in Eq. (2) becomes a sum and one simply has to sum up the array rows of χ with constant y values between $y = -b/2$ and $y = b/2$. A similar two-dimensional convolution technique has, for example, been reported by Wang and Jacques.[10]

With Monte Carlo simulations all the emitted photons, independent of the emission angle, were used to calculate $\chi(x, y)$, although the viewing angle of the experimental apparatus, see Section 3, is much smaller. This approximation is applicable because the angular distribution of remitted photons from the tissue is well described by the Lambert law.[11] Therefore, the part of the photons that reaches the experimental detector can be calculated when we know the viewing angle of the detector.

B. Color Perception

The color perception of a human observer is subjective. A quantitative description can be made using color coordinates, for which each coordinate value represents an intensity for the three primary colors (red, green, blue) remitted from the area of interest in a given scene. In addition to specifying the appropriate wavelength ranges for the three primary colors, the spectral intensity distribution of the incident light and the spectral sensitivity response of the human eye must be known. However, color perception theories based on the above approach, using, for example, the Commission Internationale de l'Éclairage (CIE) color coordinates,[12] still do not describe human color perception adequately (see Subsection 4.C). The effects of spectral intensities that emanate from all the other areas in the scene must also be included, because higher-order mental processes seem to make use of that information.

Land conducted experiments concerning the relationship between spectral light remitted from an object and its color as seen by the human observer, and he summarized his results as the so-called retinex theory.[13–15] The three main propositions of this theory are (1) The composition of light from an area in an image does not specify the color of that area. (2) The color of a unit area is determined by a trio of numbers each computed on a single wave band to give for that wave band the relationship between the unit area and the rest of the unit areas in the scene. (3) The trio of numbers, the three $\overline{R}^{\Lambda}$'s, as computed by the retinex algorithm, is the designator for the point in retinex three space, which is the color of the unit area.

This means that the spectral remission from the considered area alone does not determine its color; one must also include the remission from other areas around it. Mathematically, the retinex algorithm mentioned in the third statement is

$$R^{\Lambda}(i, j) = \sum_k \delta \log\left(\frac{I_{k+1}{}^{\Lambda}}{I_k{}^{\Lambda}}\right), \tag{3}$$

$$\delta \log\left(\frac{I_{k+1}{}^{\Lambda}}{I_k{}^{\Lambda}}\right) = \begin{cases} \log\left(\dfrac{I_{k+1}{}^{\Lambda}}{I_k{}^{\Lambda}}\right), & \left|\log\left(\dfrac{I_{k+1}{}^{\Lambda}}{I_k{}^{\Lambda}}\right)\right| > \epsilon \\ 0, & \left|\log\left(\dfrac{I_{k+1}{}^{\Lambda}}{I_k{}^{\Lambda}}\right)\right| < \epsilon \end{cases}. \tag{4}$$

In Eq. (3) I_k stands for the intensity at position k, the summation is performed over different areas along an arbitrary path from a surrounding area j to the considered area i whose color is to be determined [see Fig. 2(a)], and Λ represents the three principal wave bands, the long-wave (red), the middle-wave (green), and the short-wave (blue) regions of the visible spectrum. These wave bands correspond to the spectral sensitivity of the visual pigments.[16] In Eq. (4) ϵ is a small number that represents a threshold, ensuring that different spatial illuminations that change continuously do not influence the calculations. From Eq. (3) the $\overline{R}^{\Lambda}$'s can be calculated[14] as

$$\overline{R}^{\Lambda}(i) = \frac{1}{N} \sum_{j=1}^{N} R^{\Lambda}(i, j). \tag{5}$$

The summation in Eq. (5) [see Fig. 2(b)] is performed over a large number N of areas randomly distributed over the whole field of view. The $\overline{R}^{\Lambda}$'s represent the three values that specify a point in retinex three space, in which every point corresponds to a certain perceived color. The colors were determined by judgments of a human test group. Within retinex theory, the notion of color constancy, which stipulates that the perceived color of an object will not change markedly if the spectral composition of the illuminating light and hence the spectral remission from this object is altered, can be explained satisfactorily, since the retinex algorithms use only relative spectral remissions from the different areas involved in the image. For example, this visual phenomenon can be shown measuring the radiation from a certain object, for example, a red apple, in a scene at the three principal wave bands, and afterward changing the illumination of the scene in such a way that the remitted light from another object in the scene, say, a

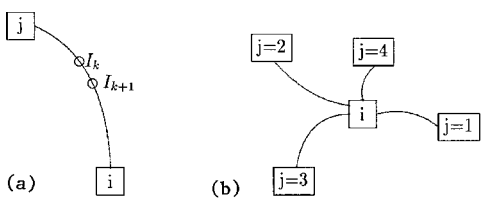

Fig. 2. Schematic representation of the summations in (a) Eq. (3) and (b) Eq. (5).

yellow banana, is the same for these three wave bands as that from the red apple. The color of the banana will not turn red but will be perceived as yellow.

In our problem of how to explain the color of a blood vessel in skin, the following approximation was made. Variations in the remission intensities from skin, along areas of a considered path that are not influenced by the vessels and along areas influenced by the vessel, are randomly distributed around an average value, with a deviation smaller than ϵ. Thus, all the terms but one in the summation of Eq. (3) disappear:

$$R^{\Lambda}(i,\ j) = \log\left(\frac{I_v{}^{\Lambda}}{I_s{}^{\Lambda}}\right), \tag{6}$$

where $I_v{}^{\Lambda}$ is the remittance of the skin above the vessel and $I_s{}^{\Lambda}$ is the average remittance from the skin not influenced by the vessel, both at a certain wave band Λ. The same result can be obtained assuming that ϵ equals zero, as $R^{\Lambda}(i,\ j)$ would depend only on the intensities at i and j. Thus, because all the $R^{\Lambda}(i,\ j)$ values are given by Eq. (6) (independent of j), the sum in Eq. (5) becomes N times $\log(I_v{}^{\Lambda}/I_s{}^{\Lambda})$ and we have

$$\overline{R}^{\Lambda}(i) = R^{\Lambda}(i,\ j) = \log(I_v{}^{\Lambda}/I_s{}^{\Lambda}). \tag{7}$$

From the three values calculated by Eq. (7) for the three wave bands, one can determine the color of the vessel in the retinex three space, resulting in the color seen by the human observer, if the retinex theory is indeed an accurate model of human color perception.

For our problem $I_v{}^{\Lambda}$ is always smaller than $I_s{}^{\Lambda}$, because absorption of blood is greater than absorption of skin at the considered wavelengths. Thus, according to Eq. (7) the $\overline{R}^{\Lambda}(i)$ values are negative. In many cases (see Table 3) the absolute values are relatively small. In this region of the retinex three space, there is a relatively small number of color points. For that reason and also because the colors printed in the retinex three space depend on the backround color of that figure, we determined the colors in the following way in this paper.

The red colors in the retinex three space are found in the region where $\overline{R}^{\Lambda}(i)$ for the short and middle wave band is small (negative) and $\overline{R}^{\Lambda}(i)$ for the long wave band is great (positive). Accordingly, the blue and green colors are obtained at great values of $\overline{R}^{\Lambda}(i)$ at the short and the middle wave bands, respectively, and for small values for the other two wave bands in each case. Therefore, if $\overline{R}^{\Lambda}(i)$ of the long (middle, short) wave band is much greater (that means less negative in our case) than $\overline{R}^{\Lambda}(i)$ of the other two wave bands, the color looks red (green, blue). When the dominance of one $\overline{R}^{\Lambda}(i)$ value is not pronounced, the color appearance is less distinct. These cases are represented by arrows in Table 3. If the $\overline{R}^{\Lambda}(i)$ for all three wavelengths are similar, turquoise-gray colors are found in the retinex three space.

Land applied Eq. (7) without explicit derivation for explaining the phenomenon of the colored shadow,[16] which can be observed when an object is placed in a long-wave beam directed to a screen. The screen is also illuminated with white light that does not interact with the object. The perceived color of the shadow of the object on the screen is blue green, which is also predicted by the retinex theory. Describing this observation with the retinex theory it is sufficient to consider the remission of the screen inside and outside the shadow.[16] Computing the colored shadow with the retinex theory is similar to the problem we discuss in this paper since there are also two areas on the surface of the skin, one that is influenced by the vessel and one that is not.

3. Materials and Methods

The experimental apparatus for the measurement of spatially resolved reflectance is shown in Fig. 3. The light beam of an arc lamp was delivered by an optical fiber (OF) to a selectable interference filter (IF). The center wavelength and bandwidth of the five filters used were 450 ± 25, 500 ± 25, 550 ± 5, 633 ± 5, and 700 ± 5 nm. The spectrally filtered light was reflected by mirror M onto the tissue or the tissue phantom. The incident light was approximately 10 deg from the normal of the sample surface avoiding image disturbance by the mirror and detection of specular reflectance. Aperture A and objective lens O (f = 50 mm) were installed in front of the CCD camera mounted above the sample. The diameter of the aperture was 2.62 mm and the distance from the sample surface to the aperture was 110 mm. The calibration of the image size relative to the object size was executed with a ruled measurement standard. The CCD camera was cooled to approximately −40 °C to improve the signal-to-noise ratio, and the image was stored in a personal computer. The active area of the CCD detector was 1024 × 1024 pixels, imaging a 4 cm × 4 cm area at the sample surface. A rectangular part of the CCD chip perpendicular to the vessel comprising 1/8 of all pixels was used to calculate the spatially resolved reflectance

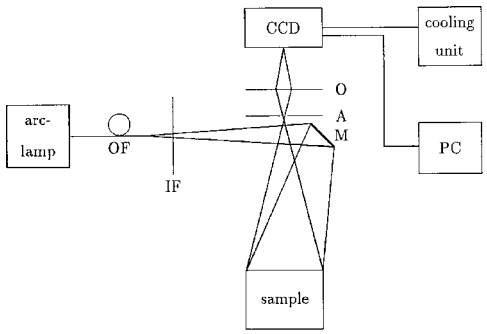

Fig. 3. Experimental arrangement for video measurement of the spatially resolved reflectance. The components are M, mirror; IF, interference filter; OF, optical fiber; O, objective; A, aperture.

profiles. At all wavelengths we measured the signal from a diffuse reflectance standard (Spectralon, average remittance of ≈99%) to correct for the spectral response of the CCD camera, and measurements of the tissue or tissue phantom were divided by the Spectralon reflectance prior to analysis. An unknown amount of specular reflection from the surface of the Spectralon is not registered by the detector. Therefore it was assumed that, together with the small amount of Spectralon absorption, there is a 5% loss of incident photons. (For Monte Carlo calculations of the liquid phantom only the diffuse reflection is regarded, because the specular reflection is not measured. For absolute measurements one also needs the number of all the photons incident upon the sample. If it is assumed that the Spectralon also produces a regular specular reflection, this part of an incident photon is not detected, because of the oblique incident beam and must, therefore, be taken into account.) Values for all the pixels with the same y coordinate (see Fig. 1) were averaged to smooth the curves. We note that this experimental setup was successfully checked with measurements on tissue phantoms using a laser as the incident source.[17]

For the tissue phantom the medium surrounding the cylindrical glass vessel was a lipid colloid (Lyposyn, 20% stock solution), which is highly scattering and has a low absorption coefficient. The Lyposyn was diluted with water to give a reduced scattering coefficient of 1 mm^{-1} at 633 nm, and 0.34% (vol/vol) oxygenated blood was added to simulate capillary blood perfusion and hence the absorption of human dermis. The absorption coefficient of the phantom liquid surrounding the model vessel is, therefore, the sum of the absorption coefficients of water and blood. Distance a from the top of the cylindrical tube to the surface of the solution was 1.4 mm. Inner diameter d of the cylinder was 1.2 mm. The wall of the glass cylinder, which was not considered in the calculations, was approximately 0.2 mm thick. Table 1 shows the reduced scattering coefficients and absorption coefficients that were used for the Monte Carlo simulations. The optical parameters of Lyposyn were measured using an established frequency domain diffuse reflectance apparatus.[18] The anisotropy parameter was set to $g = 0.8$.[19] The optical properties of blood were taken from Jacques and Keijzer[20] and van Gemert *et al.*[21] To calculate the reduced scattering coefficient of blood from the μ_s values of van Gemert *et al.,* an anisotropy factor of 0.99 was used. Assuming that a red blood cell can be approximated by a sphere, calculations based on Mie theory yielded $g = 0.995$, whereas Steinke and Shepherd[22] measured a slightly smaller value, $g = 0.985$.

Table 1. Optical Parameters for the Phantom Model[a]

Wavelength λ (nm)	Lyposyn Plus Blood		Blood	
	μ_a (mm^{-1})	μ_s' (mm^{-1})	μ_a (mm^{-1})	μ_s' (mm^{-1})
450	0.085	1.42	25	0.5
500	0.039	1.25	11.5	0.5
550	0.067	1.14	20	0.5
633	0.0022	1.00	0.5	0.5
700	0.0015	0.82	0.15/0.5*	0.5

[a]Coefficients of blood are for oxygenated blood, except for the value marked with an asterisk, which is for venous blood with oxygen saturation of 50%. The hematocrit is 40%.

The cylindrical tube was filled with whole blood. Blood was drawn directly from a vein into the heparinized cylinder to minimize contact with air and thus the possibility of increased oxygenation. Alternatively, the blood was heparinized and shaken in air to yield the oxygenated state, representative of an arterial blood sample.

Experiments on an *in vivo* vein on the ball of the thumb were performed in the same way as for the tissue phantoms. Depth a and diameter d of the vein were both estimated to be 0.5 mm, based on high resolution ultrasound measurements.

4. Results

A. Phantom Measurements

Initially we investigated the color change of the model vessel qualitatively, altering the depth of the cylindrical tube in Lyposyn and viewing it with the unassisted eye using both deoxygenated and oxygenated blood. Without a scattering medium, the deoxygenated blood had a deep red color, and oxygenated blood had a light cherry-red color. At small depths under the surface of the Lyposyn there was little change in the color of the two blood samples. Increasing the depth of the cylinders changed the appearance of the venous blood to a bluish color. At greater depths, a slight bluish hue from the oxygenated blood was seen. The influence of different amounts of oxygenated blood in the Lyposyn was also investigated. We observed that the color changes described above were more pronounced when there was more blood in the Lyposyn that surrounded the vessel.

Figures 4 and 5 show the experimental measure-

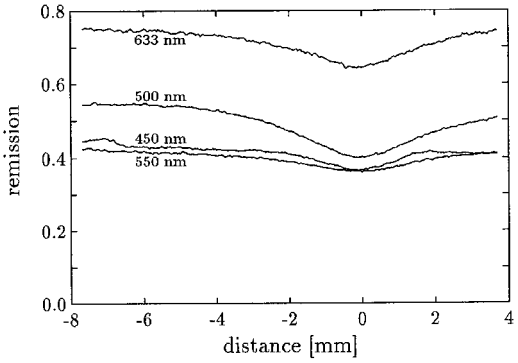

Fig. 4. Measurements of diffuse reflectance at 450, 500, 550, and 633 nm for the phantom incorporating a vessel that contains oxygenated blood.

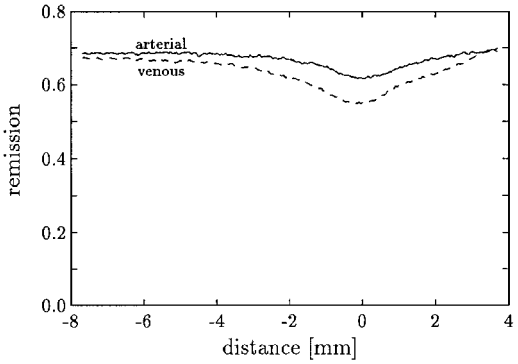

Fig. 5. Measurements of diffuse reflectance at 700 nm for the phantom incorporating a vessel. The solid curve corresponds to oxygenated arterial blood, the dashed curve corresponds to venous deoxygenated blood in the model vessel.

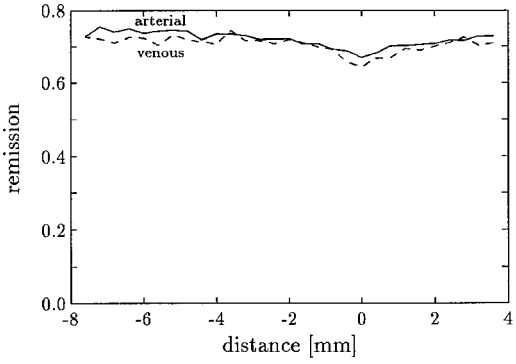

Fig. 7. Calculation of diffuse reflectance at 700 nm. The solid curve corresponds to oxygenated blood, the dashed curve corresponds to venous blood in the model vessel.

ments of the model vessel. Five measurements with oxygenated blood in the cylindrical tube at wavelengths of 450, 500, 550, 633, and 700 nm and one measurement with deoxygenated, venous blood at 700 nm were performed.

Figures 6 and 7 show the results of Monte Carlo simulations at the wavelengths corresponding to Figs. 4 and 5, using the optical parameters of Table 1 and assuming oxygenation of 50% for the venous blood. Comparison of these figures shows a general agreement of the simulations with the experimental measurements, despite some uncertainty in the optical properties of blood. The fluctuations in Figs. 6 and 7 are due to the statistical nature of the Monte Carlo simulations. The diffuse reflectances at 450 and 550 nm are less influenced by the vessel than at 500, 633, and 700 nm. The influence of the vessel on the remitted light depends not only on its absorption properties but also on the optical properties of the surrounding medium. In the case of 633- and 700-nm light the photons penetrate much deeper into the medium compared with the shorter wavelengths and, although the absorption coefficient of blood at these wavelengths is low, the longer path lengths ensure more absorption interactions with the blood vessel. In Figs. 5 and 7 we see that the greater absorption coefficient of deoxygenated blood at these longer wavelengths results in a greater decrease in diffuse reflectance above the vein.

B. *In Vivo* Measurements

In Figure 8 we display *in vivo* measurements of a vein at the inner-palm side of the thumb ball of a Caucasian male volunteer. The greatest decrease in the remission above the vein is measured at the red wavelengths. The principal reasons are the same as above; however, with *in vivo* tissue light propagation is more complex because of inhomogeneities, such as skin layers and vessel wall stratifications. A model of the skin that incorporates stratum corneum, epidermis, dermis, subcutaneous fat, underlying muscle, and the vessel should be used for the complete modeling of *in vivo* measurements. However, the optical properties of various skin layers are not well determined, and the thicknesses of the layers are known only approximately. We, therefore, used only a single homogeneous medium surrounding the vein for the Monte Carlo simulations. Table 2 shows the optical coefficients used in the Monte Carlo simulations. The optical parameters of the surrounding medium were selected to match approximately the diffuse reflectance shown in Fig. 8, as no *a priori* knowledge of the microvasculature and blood content of the tissue is available. The anisotropy factor of the tissue was assumed to be $g =$

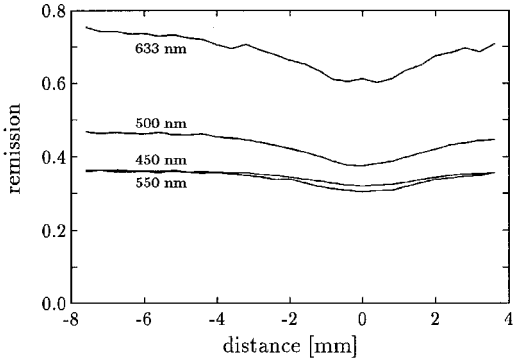

Fig. 6. Monte Carlo calculations of diffuse reflectance at 450, 500, 550, and 633 nm.

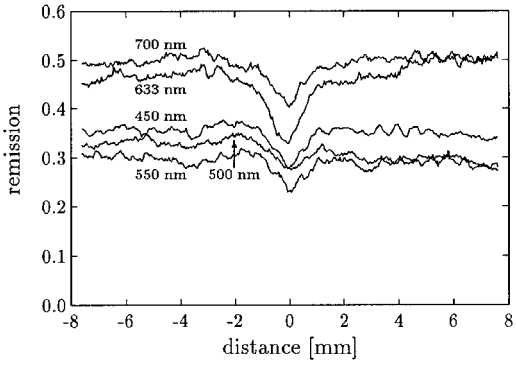

Fig. 8. Measurements of diffuse reflectance *in vivo* at 450, 500, 550, 633, and 700 nm.

Table 2. Optical Parameters used in the Monte Carlo Simulations of Diffusely Reflected Light from Skin above the Vein *in vivo*[a]

Wavelength	Surrounding Medium		Blood Vessel	
λ (nm)	μ_a (mm^{-1})	μ_s' (mm^{-1})	μ_a (mm^{-1})	μ_a' (mm^{-1})
450	0.18	3.0	25	0.5
550	0.15	2.0	20	0.5
633	0.025	1.0	0.5/1.75*	0.5

[a]The values of blood at 450 and 550 nm and the reduced scattering coefficient at 633 nm are the same for oxygenated and deoxygenated blood and were taken from Table 1. The absorption coefficient at 633 nm marked by an asterisk is for venous blood, assuming a saturation of 50%, and the value without the asterisk is for oxygenated blood.

0.9.[2] The calculations were made at 450, 550, and 633 nm, representing the short-, the middle-, and the long-wavelength ranges alluded to in the description of the retinex theory.

In Fig. 9 the simulation results for 450, 550, and 633 nm can be seen. Using the optical properties of Table 2 we were able to calculate the light propagation for the model vessel and the *in vivo* vessel, compare the model predictions with measured spectra, and interpret the results qualitatively. However, the resulting skin colors as seen by a human observer are not obvious from this. In Fig. 8, for example, although there is a great decrease in the red wavelengths, more red light than blue light is still reflected above the vein, but the vein is not perceived as red.

C. Retinex Theory

For a full description of the observed colors the three $\overline{R}^{\Lambda}$'s have to be calculated and looked up in retinex three space, also called lightness space, to obtain the perceived color of the vessel. Using Eq. (7) the remission above the vessel and at locations not influenced by the vessel have to be determined at wave bands defined by the color sensitivity of the eye. However, we have made measurements only at single wavelengths. To evaluate whether these

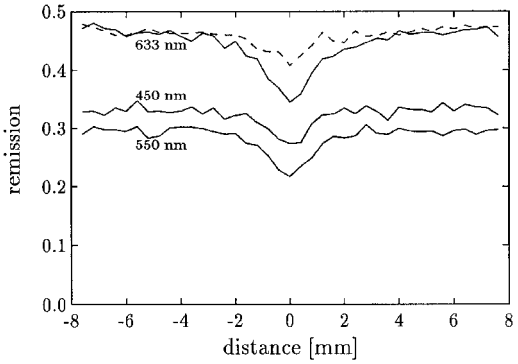

Fig. 9. Simulations of the *in vivo* vessel at 450, 550, and 633 nm. At 633 nm the dashed curve represents arterial blood and the solid curve represents venous blood. Depth a of the blood vessel is 0.5 mm, and the diameter is also 0.5 mm.

are sufficient to determine the perceived color of the vessel, we made Monte Carlo simulations as shown in Fig. 9 from 400 to 650 nm in 25-nm steps. The absorption coefficients at the different wavelengths were calculated based on known values of oxygenated blood.[20,21] The reduced scattering coefficients were interpolated from Table 2. The $\overline{R}^{\Lambda}$'s were computed using the simulation results and the spectral sensitivity functions of the retinal cones.[16] We were, thereby, able to calculate what would be measured if we could use the wave bands determined by the cones and to compare this with the results at single wavelengths. From these calculations the following results were obtained. For the short, medium, and long wave bands, $\overline{R} = -0.088$, $\overline{R} = -0.126$, and $\overline{R} = -0.127$, respectively. These correspond well with the values at 450, 550, and 633 nm from Fig. 9 for venous blood, which are $\overline{R}^{450} = -0.07$, $\overline{R}^{550} = -0.12$, and $\overline{R}^{633} = -0.13$. These latter values were calculated according to Eq. (7), where I_v^{Λ} is the remittance above the vessel and I_s^{Λ} is the average remittance beside the vessel given in Fig. 9. For example, for $\lambda = 550$ nm, $I_v^{550} = 0.22 \pm 0.01$ and $I_s^{550} = 0.29 \pm 0.01$. The error of I_s^{550} was computed from the fluctuations of the Monte Carlo simulations in Fig. 9 for the remission values that are not influenced by the vessel. The same absolute error was assumed for I_v^{550}. From this one has $\overline{R}^{550} = \log(I_s^{\Lambda}/I_v^{\Lambda}) = -0.12 \pm 0.02$. For the other wavelengths in this figure and for the curves in the other figures we get approximately the same errors. These errors have no significant influence on the determination of the color of the vessels, because the number of colors shown in retinex lightness space are relatively small and, thus, the determination of the color is within a certain range qualitatively.

Therefore, at least in this case, it is possible to use the three wavelengths at 450, 550, and 633 nm instead of using the wave bands that correspond to the spectral sensitivity functions of the eye. Hence, in the following we apply these three wavelengths to represent the short, middle, and long wave bands of the retinex theory.

The lightness values for the data shown in Fig. 8 are $\overline{R}^{450} = -0.06$, $\overline{R}^{550} = -0.10$, and $\overline{R}^{633} = -0.16$, which means that $\overline{R}^{550}$ and $\overline{R}^{630}$ are almost two and three times smaller than $\overline{R}^{450}$. According to Subsection 2.B these values specify a blue color, which corresponds with observation. (We also applied CIE color space calculations[23] to derive the color of the *in vivo* vein using all the wavelengths shown in Fig. 8. The color of the tissue both above the vein and of the surrounding tissue was determined to be without a distinct hue according to this theory. In addition, the locations calculated for the colors in this color space were close together. Thus, no distinct color change could be determined.) These lightness values for the *in vivo* vein differ from the results of the calculation shown above because the Monte Carlo simulation does not match the measurement exactly.

The consequence of this is that the color of the vein according to the simulations is between blue and turquoise.

In Fig. 9 the dashed curve shows the remission when the vessel is filled with oxygenated blood at 633 nm. At 450 and 550 nm, oxygenated and deoxygenated blood have approximately the same optical coefficients. Therefore the lightness values are $\overline{R}^{450} = -0.07$, $\overline{R}^{550} = -0.12$, whereas $\overline{R}^{633}$ changes to -0.06. The lightness values for the oxygenated vessel at 633 nm are nearly the same as at 450 nm. We specify a turquoise color for these values. The overall attenuation is less compared to the vein, producing a color that is less saturated than that of the vein.

It is possible to perform simulations for all the desired depths and diameters of the vessel and calculate from these the corresponding color appearance. Table 3 summarizes the parameters of the *in vivo* vein, the two simulations above, and the additional simulations that are discussed below. Simulation 3 shows that changing the diameter from $d = 0.5$ mm (No. 1) to $d = 0.8$ mm and keeping the center of the vessel at a constant depth results in larger absolute lightness values and in a greater decrease of $\overline{R}^{630}$ than of $\overline{R}^{450}$, which means that the color shifts to the blue region.

Next we investigated how the color of the vein with 50% oxygenated blood changes when it is closer to the surface. As in Fig. 9, we used a diameter of 0.5 mm, but depth a was changed to 0.2 and 0.04 mm. The diffuse reflectance calculated by the Monte Carlo simulations can be seen in Figs. 10 and 11, and the resulting lightness values are listed in Table 3 (Nos. 4 and 5, respectively). As expected, the closer to the surface the greater the influence of the vessel on the remission, and hence the greater the absolute lightness values. For superficial vessels, photons

Table 3. Parameters of the *in vivo* Vein Measurement and the Vessel Simulations[a]

Simulation No.	a (mm)	d (mm)	$\overline{R}^{450}$	$\overline{R}^{550}$	$\overline{R}^{633}$	Color
0	≈0.5	≈0.5	−0.06	−0.10	−0.16	Blue**
1	0.50	0.50	−0.07	−0.12	−0.13	Turquoise → blue
2	0.50	0.50	−0.07	−0.12	−0.06	Turquoise*
3	0.35	0.80	−0.17	−0.23	−0.33	Turquoise → blue
4	0.20	0.50	−0.31	−0.38	−0.26	Turquoise → red
5	0.04	0.50	−0.82	−0.88	−0.34	Turquoise ⇒ red
6	0.04	0.50	−0.82	−0.88	−0.14	Violet, dark red*
7	0.04	0.24	−0.48	−0.50	−0.14	Violet, dark red

[a]The *in vivo* vein measurement is indicated by a double asterisk. Vessels that represent arteries are marked by an asterisk, the others are for veins.

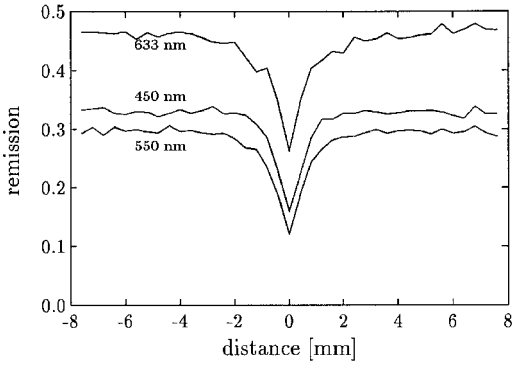

Fig. 10. Monte Carlo simulations for diffuse reflectance of a vein with $a = 0.2$ mm and $d = 0.5$ mm for different wavelengths.

at 450 and 550 nm were more influenced by the presence of the vein than at 633 nm. The lightness value at 450 nm thus becomes greater than at 633 nm, so the color of these veins tends to become red, indicated by arrows in Table 3. Hence, some minimum depth below the skin surface is necessary for a vein to display its characteristic bluish color. In Fig. 11 the calculated remission of an arterial vessel at 633 nm is also shown (dashed curve). Its remission at this wavelength is much less affected by the vessel than for the venous case. The lightness value in the long wave band is $\overline{R}^{633} = -0.14$ (No. 6 in Table 3). According to the retinex theory, a dark red to violet color is predicted.

Additional simulations for a superficial vein at $a = 0.04$ mm, but with a smaller diameter of $d = 0.24$ mm, were performed (No. 7 in Table 3). Compared with the vein with $d = 0.5$ mm and $a = 0.04$ mm (No. 5), all the absolute lightness values are smaller but the long-wavelength value is decreased relatively more. These values are also in the reddish region of the color space. Thus, in addition to the minimum depth requirement, a minimum vessel diameter is needed for a vein to look blue. This explains why the normal capillary bed does not look blue, even at low oxygen saturation of the blood.

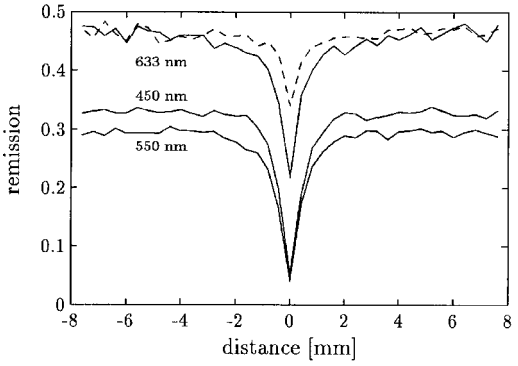

Fig. 11. Monte Carlo simulations for diffuse reflectance of a vein with $a = 0.04$ mm and $d = 0.5$ mm for different wavelengths. Data for 100% oxygenation saturation at 633 nm are also shown (dashed curve).

Another interesting feature can be seen by comparing the apparent diameter of the vein in Figs. 9, 10, and 11, showing vessels of $d = 0.5$ mm, at different depths below the skin surface of $a = 0.5$ mm, $a = 0.2$ mm, and $a = 0.04$ mm, respectively. We see that the apparent diameter, defined by the width at the half-peak value of the remission curve, changes from 1.7 to 1 to 0.7 mm. Thus, the deeper the vessel, the greater its apparent diameter. At a depth of $a = 0.5$ mm the apparent diameter is more than three times the real diameter. Considering the above size and depth requirements for a vein to look blue, this result implies that a certain minimum area on the surface of the skin must be affected by the vein's presence. In addition to the purely photometric effects seen in Fig. 9, this minimum area requirement plays a role in the retinex calculation through the latter's dependence on the ratio of the spectral remissions from the area of the object to that from the surrounding areas. This implies that for deeper and larger veins the total observed area needs to increase to obtain the typical bluish color.

5. Discussion and Conclusions

To summarize, the reason for the bluish color of a vein is not greater remission of blue light compared with red light; rather, it is the greater decrease in the red remission above the vessel compared to its surroundings than the corresponding effect in the blue. At first it seems astonishing that red light is more attenuated above the vessel than blue light, since, as Table 1 shows, the absorption of blood is much less in the red than in the blue. This is the result of the spectral characteristics of light propagation in tissue. Blue light does not penetrate as deeply into tissue as red light. Therefore, if the vessel is sufficiently deep, the reflectance in the blue will be affected to a lesser extent. Deoxygenated venous blood has a greater absorption coefficient than oxygenated arterial blood in the red spectral region, and this difference of two, rather small, values is amplified because of the long path length of red light in scattering tissue. As a result, veins are more likely to look blue than arteries at the same diameter and depth. Often arteries are not seen at all because they are generally smaller than veins and have thicker vessel walls. It has been shown that a small vessel will look red when close to the surface. However, if a superficial vessel is large it can still look bluish, particularly in the case of the vein. On the other hand, if the depth of a vessel is large, even red remitted light will not be influenced by the vessel, and it will not be seen. We note that, for the calculations here, we assumed an oxygen saturation of 50% for venous blood. This is somewhat arbitrary, but other possible realistic values do not change the conclusions.

As shown in Fig. 8, even above the vein more red than blue light is remitted. Thus, for a complete explanation of the perceived color of the vessel one needs the retinex theory. With the retinex theory the color can be determined by the relative intensities at the three wave bands from a particular scene compared to the surrounding area. The intensities of these wave bands are weighted by spectral functions that represent the human spectral vision. In this study we used single wavelengths that are representative of these spectral functions, and, therefore, a retinex color three space based on selected wavelengths should be applied. However, we chose typical wavelengths for the long-wave, middle-wave, and short-wave regions and made qualitative estimates of the colors. Therefore, we believe that we are justified in applying the usual retinex three-color space. In one example, we calculated the remission at several wavelengths and used the spectral sensitivity of the cones to show that the approach of using only three single wavelengths is justified.

It is interesting to speculate whether retinex theory is necessary for other color perception issues in medicine (e.g., the color of port-wine stains, vitiligo lesions, blue nevi, age spots, eyes, hair), or whether the perceived color can be simply related to the absorption spectra of chromophores, possibly modified by the presence of light scattering and measured with a reflectometer. If the problem of vessel color is any guide, it seems that retinex theory may provide an essential step in the description of color perception.

Alwin Kienle gratefully acknowledges the financial support of a doctoral scholarship from the German Academic Exchange Service. We also acknowledge support from the Ontario Laser and Lightwave Research Center, Toronto, for this study.

References

1. R. R. Anderson, "The physical basis of brown skin colors (melanoderma)," in *Brown Melanoderma,* T. B. Fitzpatrick, M. M. Wick, and K. Toda, eds. (University of Tokyo, Tokyo, 1986), pp. 4–7.
2. W. Cheong, S. A. Prahl, and A. J. Welch, "A review of the optical properties of biological tissues," IEEE J. Quantum Electron. **26,** 2166–2185 (1990).
3. A. Kienle, L. Lilge, M. S. Paterson, B. C. Wilson, R. Hibst, and R. Steiner, "Investigation of multi-layered tissue with *in vivo* reflectance measurements," in *Photon Transport in Highly Scattering Tissue,* S. Avrillier, B. Chance, G. J. Mueller, A. V. Priezzhev, and V. V. Tuchin, eds., Proc. Soc. Photo-Opt. Instrum. Eng. **2326,** 212–221 (1994).
4. V. Twersky, "Absorption and multiple scattering by biological suspensions," J. Opt. Soc. Am. **60,** 1084–1093 (1970).
5. A. Ishimaru, *Wave Propagation and Scattering in Random Media* (Academic, New York, 1978), Chap. 7 and Chap. 3, p. 66.
6. Y. Kuga and A. Ishimaru, "Retroreflectance from a dense distribution of spherical particles," J. Opt. Soc. Am. A **1,** 831–835 (1984).
7. R. L. Gregory, *Eye and Brain: the Physiology of Seeing* (Princeton U. Press, Princeton, N.J., 1990), Chap. 8.
8. F. P. Bolin, L. E. Preuss, R. C. Taylor, and R. J. Ference, "Refractive index of some mammalian tissue using a fiber optic cladding method," Appl. Opt. **28,** 2297–2303 (1989).
9. B. C. Wilson and G. Adam, "A Monte Carlo model for the

absorption and flux distribution of light in tissue," Med. Phys. **10,** 824–830 (1983).
10. L. Wang and S. L. Jacques, *Monte Carlo Modeling of Light Transport in Multi-layered Tissues in Standard C* (University of Texas M. D. Anderson Cancer Center, Houston, Tex., 1992).
11. A. Kienle, "Lichtausbreitung in biologischem Gewebe," thesis (University of Ulm, Ulm, Germany, 1994).
12. D. L. MacAdam, *Color Measurements: Themes and Variations* (Springer-Verlag, Berlin, 1985), Chap. 3.
13. E. H. Land and J. J. McCann, "Lightness and retinex theory," J. Opt. Soc. Am. **61,** 1–11 (1971).
14. E. H. Land, "Recent advances in retinex theory," Vision Res. **26,** 7–21 (1986).
15. E. H. Land, "An alternative technique for the computation of the designator in the retinex theory of the color vision," Proc. Natl. Acad. Sci. U.S.A. **83,** 3078–3080 (1986).
16. E. H. Land, "The retinex theory of color vision," Sci. Am. **237,** 108–128 (1977).
17. A. Kienle, L. Lilge, M. S. Paterson, B. C. Wilson, R. Hibst, and R. Steiner, "Spatially resolved absolute diffuse reflectance measurements for remote determination of the optical properties of biological tissue," Appl. Opt. **35,** (to be published).
18. B. C. Wilson, M. S. Patterson, and B. W. Pogue, "Instrumentation for *in vivo* tissue spectroscopy and imaging," in *Medical Lasers and Systems II,* D. M. Harris and C. M. Penney, eds., Proc. Soc. Photo-Opt. Instrum. Eng. **1892,** 132–147 (1993).
19. H. J. van Staveren, C. J. M. Moes, J. van Marie, S. A. Prahl, and M. J. C. van Gemert, "Light scattering in Intralipid-10% in the wavelength range of 400–1100 nm," Appl. Opt. **31,** 4507–4514 (1991).
20. S. Jacques and M. Keijzer, "Dosimetry for lasers and light in dermatology: Monte Carlo simulations of 577 nm pulsed laser penetration into cutaneous vessels," in *Lasers in Dermatology and Tissue Welding,* O. T. Tan, R. A. White, and J. V. White, eds., Proc. Soc. Photo-Opt. Instrum. Eng. **1422,** 2–13 (1991).
21. M. J. C. van Gemert, J. W. Pickering, and A. J. Welch, "Modelling laser treatment of port-wine stains," in *Management and Treatment of Benign Cutaneous Vascular Lesions,* O. T. Tan, ed. (Lea & Febiger, Philadelphia, 1992), pp. 24–47.
22. J. M. Steinke and A. P. Shepherd, "Comparison of Mie theory and the light scattering of red blood cells," Appl. Opt. **27,** 4027–4033 (1988).
23. M. Richter, "Farbmetrik," in *Optik,* L. Bergmann and C. Schäfer, eds. (Walter de Gruyter, Berlin, Germany, 1978), pp. 641–699.